Water Science and Engineering 2021, 14(1): 72−79

HOSTED BY

ELSEVIER

Available online at www.sciencedirect.com

Water Science and Engineering

journal homepage: wse.hhu.edu.cn

Analytical solution for a strong free-surface water vortex describing flow in a full-scale gravitational vortex hydropower system

Vladimir Joel Alzamora Guzmán, Julie Anne Glasscock*

Energy Research Group, Kadagaya Research Centre for Appropriate Technology, Junin 12866, Peru

Received 21 September 2020; accepted 4 January 2021
Available online 29 March 2021

Abstract

Strong free-surface water vortices are found throughout industrial hydraulic systems used for water treatment, flow regulation, and energy generation. Previous models using the volumetric flow rate as a model input have generally been semi-empirical, and have tended to have some limitations in terms of the design of practical hydropower systems. In this study, an analytical model of a strong free-surface water vortex was developed. This model only requires the water head and geometric parameters as its inputs and calculates the maximum volumetric flow rate, air-core diameter, and rotational constant. Detailed experimental depth−discharge data from a full-scale gravitational vortex hydropower system, unavailable in the relevant literature, were obtained, and the simulated results showed excellent agreement with the experimental observations. These data could be used to verify similar models using laboratory-scale physical models in order to investigate the scaling effects. In contrast to previous models, this model does not assume a constant average velocity across the vortex radius and allows precise calculation of the resultant velocity vectors. Therefore, this model presents advantages in turbine design for energy generation systems.

Keywords: Gravitational vortex; Velocity measurements; Scalability; Analytical model; Microhydropower

1. Introduction

Strong free-surface vortices are extensively used in industrial-scale hydraulic engineering for water treatment and flow control (Knauss, 1987), and, more recently, for energy generation (Alzamora Guzmán et al., 2019). Vortex formation is commonly achieved using the combination of an open rectangular inlet channel and a scroll-type circulation tank. These facilities induce strong vortices in the tank center when water exits through a hole in the floor. The vortex flow is considered strong when a stable air core develops. The steady spiraling water flow in the vortex increases the rotation and velocity, which is useful for energy generation.

The gravitational vortex hydropower (GVHP) system is a relatively new technology that operates at a low head and high flow rates and is suitable for off-grid and distributed energy systems. The technology has been shown to be economically and technically feasible, especially for application in developing countries, compared to other alternative renewable and non-renewable energy sources (Dhakal et al., 2015). Compared to traditional large-scale hydroelectric systems, GVHP has a much lower impact on the surrounding ecosystem as construction of a large dam is not necessary. Only a fraction of the river flow is diverted and passes through the system, and all water is returned downstream to the river. However, the fraction of diverted water and the extent of in-river infrastructure are highly site-specific. Several companies have commercialized the GVHP technology at various scales (Kouris, 2000; Turbulent, 2020; Vorteco, 2016; Zotlöterer, 2004). The state-of-the-art installations of GVHP technology and related challenges and opportunities have been discussed in a recent review article (Timilsina et al., 2018).

In the GVHP system, to extract the kinetic energy from the water vortex, a turbine is placed in the tank center at the point

* Corresponding author.
E-mail address: julie@kadagaya.org (Julie Anne Glasscock).
Peer review under responsibility of Hohai University.

https://doi.org/10.1016/j.wse.2021.03.004

of maximum vortex rotation. For the full-scale systems currently installed around the world, the average total efficiency is around 55% (Timilsina et al., 2018). In such systems, most efficiency losses are related to the interaction between the turbine and the vortex. The low turbine efficiency has been recognized as a limitation of this technology, and many groups have investigated different turbine designs, both via modeling (Khan, 2016; Nishi and Inagaki, 2017; Wanchat and Suntivarakorn, 2011) and experimental studies (Power et al., 2016; Rahman et al., 2016; Sritram et al., 2015). Given that the three-dimensional (3D) flow field in a water vortex is highly complex, it is difficult to describe and predict these interactions. The turbine efficiency is closely related to the inlet and outlet velocity triangles. Hence, to design a more efficient turbine, it is necessary to describe the water vortex in detail. In addition, the geometrical parameters of the circulation tank need to be optimized to maximize the strength of vortex formation (Mulligan et al., 2016).

A safe and effective hydraulic design requires knowledge of the tangential velocity profile of the strong free-surface vortex. Various analytical models of the tangential velocity have been proposed. Although developed nearly 150 years ago, the Rankine model (Rankine, 1872) has proved to be a workable solution and is still commonly used today. Other models (Mulligan et al., 2018; Vatistas et al., 2015) have been presented more recently and have shown agreement with experimental results. Mulligan et al. (2018) extensively investigated the effect of the geometric parameters and inlet flow conditions and compared the depth−discharge relationship derived from various models (Mulligan et al., 2016) and a single available experimental dataset for a full-scale vortex system (Drioli, 1969). The results of the compared models showed similar trends, but a large variation in values. Due to the major lack of experimental data from full-scale vortex systems, most previous models were verified using laboratory-scale physical models of circulation tanks, and their applicability to full-scale systems has not generally been verified. A major limitation of most previous models is that they require the volumetric flow rate (Q) as an input variable. Given that there is a complex relationship between the geometric parameters and Q, a detailed investigation of the geometrical parameter space requires experimental measurement of Q values as the model input. Hence, the model input already contains some experimental uncertainty, and fully analytical models have not yet been presented. Although the models have been experimentally verified using small-scale laboratory test set-ups, these systems could be susceptible to surface tension and viscosity effects that are negligible in large systems. In addition, hydraulic structures where large vortex formations occur often have significantly high Reynolds numbers, and the vortex formation could be affected by turbulent flow (Mulligan et al., 2016). Such conditions may not be accurately described by semi-analytical and empirical models that are verified by laboratory-scale physical models.

To overcome the limitations of previous models for practical application to full-scale systems, this study developed an improved analytical model. The major improvement is that Q is not required as an input. In addition, the weighted average velocity is calculated by the vortex radius rather than by assuming a constant value. This allows estimation of the exact position of the resultant velocity vector. The proposed model is expected to be useful in the design of a turbine that interacts with vortex flow in energy generation systems such as GVHP. As computational resources become faster and cheaper, numerical methods such as computational fluid dynamics (CFD) are increasingly being used to model vortex fields (Kueh et al., 2014; Li et al., 2008; Mulligan, 2015). Although velocity vectors can be obtained from CFD simulations, detailed verification using physical models is required before the output can be used for design purposes, especially for large-scale commercial systems. In contrast to other studies, this study verified the analytical results using experimental data from a full-scale system rather than laboratory-scale prototypes.

2. Methods

2.1. Analytical model

Fig. 1 shows schematic diagrams that define the geometric variables of the scroll-type circulation tank, in which a water vortex is formed. Fig. 1(a) shows a cross-section of the tank and the water surface defined by the vortex, where h is the water head (m) and a is the diameter of the air core (m). Fig. 1(b) displays a top view of the tank and the geometric variables that were previously defined (Mulligan et al., 2015). In this figure, b is the inlet channel width (m), b_i is the width of the inlet section of the channel to the tank (m), D_e is the effective tank diameter (m), R_i is the inlet radius (m), and d is the diameter of the exit hole in the tank floor (m). In most cases, b_i is equal to b when the inlet channel delivers water flow directly into the tank. However, b_i is less than b in the case where an inlet reduction is used, as shown by the narrow grey line along the dashed D_e curve in Fig. 1(b). In this study, the GVHP system for the experimental verification of the model was a 10-kW-scale plant, which has been previously described in detail (Alzamora Guzmán et al., 2019). The system has dimensions of $b = 1.65$ m, $R_i = 3$ m, $D_e \approx 5$ m, and $d = 1.4$ m, and b_i can vary. The typical range of h is 0.8−1.4 m.

Detailed evaluations of the effect of the tank geometry on vortex behavior have been performed (Mulligan, 2015; Mulligan et al., 2016; Power et al., 2016), and are outside the scope of this study. These studies showed that optimization of the geometrical parameters are important for maximizing the vortex strength and achieving a high power output from the GVHP system. Therefore, it is critical to optimize the tank and turbine geometry during the design phase. Current models that require Q as an input are unable to perform a full parameter optimization and can introduce uncertainty because the Q values are experimentally determined. Given that it is impractical to measure the Q values for a range of geometrical parameters in full-scale systems (with the fixed geometry of a circulation tank), it is highly beneficial to have a fully analytical solution that provides Q as an output.

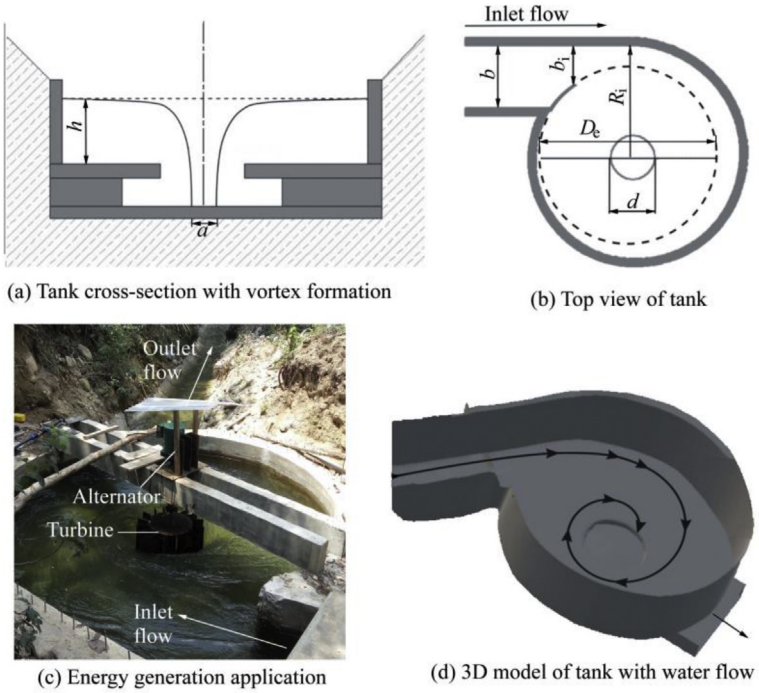

(a) Tank cross-section with vortex formation

(b) Top view of tank

(c) Energy generation application

(d) 3D model of tank with water flow

Fig. 1. Schematic diagrams defining geometrical variables of a circulation tank in which a vortex is formed, photograph of a system used for energy generation, and a 3D tank model with water flow indicated by arrows.

To develop an improved analytical model, this study used Bernoulli's equation to describe the conservation of energy with the assumption of an incompressible fluid (i.e., a constant density ρ) (Bansal, 2010), which is shown in Eq. (1):

$$\frac{v^2}{2g}+\frac{p}{\rho g}+z=c \tag{1}$$

where v is the velocity (m/s), g is the acceleration due to gravity, p is the pressure (MPa), ρ is the density of water, z is the potential energy per unit head, and c is a constant. The first term on the left side of Eq. (1) is the kinetic energy per unit of kinetic head, and the second term refers to the pressure energy per unit of pressure head. According to the law of energy conservation, the sum of these two terms and z is a constant. Thus, Eq. (1) can be rewritten to describe h (m), which is expressed as follows:

$$h=\frac{v_\theta^2}{2g}+\frac{w^2}{2g}+\frac{p}{\rho g} \tag{2}$$

where v_θ and w represent the tangential velocity (m/s) and axial velocity (m/s), respectively. The first two terms on the right side of Eq. (2) denote the kinetic energy terms from the tangential velocity and the axial velocity, respectively. Here, h is defined with respect to the bottom of the tank at $z=0$, and thus h becomes zero. At the air−water interface at the base of the GVHP tank, p and w are assumed equal to zero, and the maximum tangential velocity $v_{\theta\mathrm{m}}$ (m/s) occurs at this point (i.e., at a radius of $a/2$). Hence, Bernoulli's equation can be written as follows:

$$v_{\theta\mathrm{m}}=\sqrt{2gh} \tag{3}$$

We believe that the assumption of free discharge is appropriate for the GVHP system. As shown in Fig. 1(a), the tank is designed with a large sub-floor volume to ensure free discharge of water from the tank. The system was tested under various flow conditions for several years, and a full air core was always observed with no water backup or other evidence of restricted discharge. In addition, as discussed later, the air-core diameter predicted by the model using this assumption was consistent with the experimental observations.

The ideal or irrotational model for a free-surface vortex was used to describe the tangential velocity, which is expressed as follows:

$$v_\theta=\frac{\Gamma}{2\pi r(x)} \tag{4}$$

where Γ is the rotational constant (m^2/s), and $r(x)$ is the radius at distance x from the center of the tank at which v_θ is calculated (m). Here, Γ is a constant value anywhere within the vortex, and it is given as follows:

$$\Gamma=v_{\theta\mathrm{m}}\pi a \tag{5}$$

To avoid assuming an average tangential velocity, the weighted average tangential velocity at the inlet v_i (m^2/s) was calculated using measure theory (Tao, 2011) to enable numerical integration, which is expressed as follows:

$$v_i = \frac{\int_0^N [v_\theta r(x) + \tau/2]\mathrm{d}\mu}{\int_0^N [r(x) + \tau/2]\mathrm{d}\mu} \tag{6}$$

where τ is the precision of the analysis (0.000 1), μ is the integer counter, and N is defined as the upper limit of the integration, and N is estimated as follows:

$$N = \frac{(x_1 - x_0)}{\tau} \tag{7}$$

where x_0 and x_1 are the lower and upper boundaries of the analysis range of the distance (m), respectively. The function $r(x)$ as shown in Eq. (6) is the radius formulated in a way to make numerical integration possible, which is expressed as follows:

$$r(x) = \mu\tau + x_0 \tag{8}$$

In the specific case of the inlet velocity, $x_0 = R_i - b_i$ and $x_1 = R_i$, Bernoulli's equation is used to calculate w, and the conditions of cyclostrophic balance are expressed as follows:

$$p = -\frac{v_\theta^2[r(x) - a/2]\rho}{r(x)} \tag{9}$$

As for the tangential velocity, the weighted average of the axial velocity at the outlet w_o (m/s) is calculated by combining Eqs. (6) and (7) with $x_0 = a/2$ and $x_1 = d/2$, where w_o is expressed as follows:

$$w_o = \frac{\int_0^N [wr(x) + \tau/2]\mathrm{d}\mu}{\int_0^N [r(x) + \tau/2]\mathrm{d}\mu} \tag{10}$$

Finally, the volumetric flow rates at the inlet (Q_i) and outlet (Q_o) are respectively calculated by Eqs. (11) and (12):

$$Q_i = hb_i v_i \tag{11}$$

$$Q_o = w_o A \tag{12}$$

where A is the cross-sectional area of the inlet channel (m^2). Afterward, the algorithm is solved using the constant-volume assumption of equal inlet and outlet discharges ($Q_i = Q_o$).

The repeatability and sensitivity of the model to uncertainties in the model input were also analyzed. The model sensitivity was quantified by varying the input parameters over a range of fractions to simulate uncertainties in the input parameters, and by observing the effect of the input parameters on the output parameters. Scatter plots were produced to identify the dependences between inputs and outputs.

2.2. Experiments

To obtain the depth−discharge plots for verification of the analytical model, the volumetric flow rate was experimentally measured under different head conditions (0.8−1.1 m) in the full-scale GVHP system, which was previously described in Alzamora Guzmán et al. (2019). All measurements were performed without a turbine in place as the fundamental behavior of the vortex was of interest in this study. A velocity sensor was constructed using a computer fan (92 mm in diameter) with an inbuilt Hall sensor to measure the water velocity. This velocity sensor was first calibrated by establishing a relationship with the output voltage of the device, which is proportional to the rotational speed of the fan, and water surface velocity. The output of the velocity sensor was first measured by placing it close to the water surface (submerged to a depth sufficient to just cover the fan). To obtain a reference value to calibrate the velocity sensor, the float method was used to measure the surface velocity, in which the time taken for a float to travel over a distance of (3.15 ± 0.05) m in the inlet channel was determined. The velocity estimated by the velocity sensor was then calibrated against the float-method-based surface velocity measurement. Twelve repeated measurement runs were performed to obtain the average and standard deviation. Thereafter, subsequent velocity measurements were performed by the calibrated velocity sensor at a depth of $h/2$ and in the channel center ($b/2$). Over the cross-sectional area of the inlet channel (A in Eq. (12)), it is reasonable to assume that the velocity varies horizontally and vertically because of the effect of channel walls. Preliminary measurements showed that this variation was not significant and fell within the experimental uncertainty. However, the cross-section center that is away from the walls and water surface was chosen to perform velocity measurements, because it was assumed to represent the average velocity most accurately. Fig. 2 shows a schematic diagram of the experimental setup for the velocity measurements. An algorithm was used to calculate the real-time average velocity as the data was collected using an Arduino Uno microcontroller with a sampling rate of 0.1 s per measurement. The final velocity measurements were determined over a period of approximately 60 s. Velocity measurements were conducted in the inlet channel, with a constant b of 1.65 m (before the region with the inlet reduction of the channel), and Q_i was determined according to Eq. (11). Experimental values were determined for various h and b_i

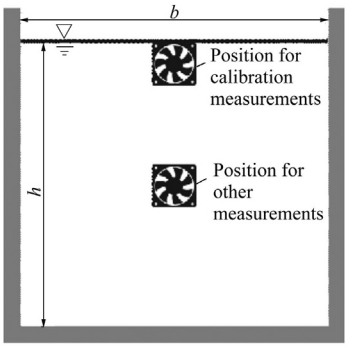

Fig. 2. Schematic diagram of experimental setup for velocity measurements (the grey areas indicate the walls of the tank).

conditions and were compared to the values calculated by the model for the same conditions.

3. Results and discussion

3.1. Model validation

Fig. 3 shows the three main outputs of the model, namely, Q, a, and Γ, as a function of h for the geometrical parameters of the full-scale GVHP system (d = 1.40 m, b = 1.65 m, and R_i = 3 m). The generated data points for each set of conditions (using h, d, b_i, and R_i as inputs) resulted in smooth curves. A repeatability analysis was performed, in which the model was run ten times using the same input values. The model outputs were obtained with a resolution of 16 decimal places, and identical output values were obtained every time. Hence, rounding errors and other computational uncertainties were considered insignificant. As shown in Fig. 3, Q and Γ increased with increasing h, and a tended to slightly decrease with increasing h.

To quantitatively verify the model accuracy, the experimental and calculated volumetric flow rates for various head and inlet width values were compared under the conditions of d = 1.40 m and R_i = 3 m (Fig. 4). The error bars in Fig. 4 represent the propagated uncertainties from the entire experimental process. To easily compare the test cases, the Q values were grouped by b_i. In all cases, the real width was less than the inlet channel width ($b_i < b$). As shown in Fig. 4, the experimental and analytical results showed identical values within experimental uncertainty for the conditions tested here. The main source of experimental errors came from velocity measurements (4%−6%), and the measurements of head and other geometrical parameters accounted for 1% and less than 0.5% of total uncertainty, respectively. These sources presented a total uncertainty of approximately 5% after error propagation calculations. Hence, the accuracy of the proposed model for describing vortex flow in a large-scale system was verified. An additional experimental verification of the model could be achieved by measuring a. However, Q was chosen as the main verification parameter because it can be more accurately measured than a. As indicated in Fig. 3(b), a merely varied by 10% over the measured head range. Therefore, it is difficult to experimentally measure a with sufficient precision for an accurate comparison with the analytical data. However, from photographs taken from above the exit annulus, an air-core diameter of around 1 m was approximated for all head conditions, which was consistent with the analytical results.

During the experimental measurements using the full-scale GVHP system, some interesting phenomena were observed. When b_i was changed, a slight shift of the air core center was observed, which resulted in eccentricity between the air core and exit annulus. In the GVHP tank, the position of the exit annulus is fixed, whereas changes in b_i lead to slight changes in D_e and the position of the vortex in the tank. Under ideal laboratory conditions, the position of the exit annulus can be easily altered to ensure the concentricity with the air core. However, this is difficult in the full-scale system. This aspect might introduce some experimental uncertainties. In addition, under the condition of low river flow in the dry season, insufficient amounts of water enter the channel to achieve the maximum flow rate. When the measurements of Q versus h were performed under these conditions, it was found that Q linearly increased with the rise of h, and the experimental data followed the simulated curve quite well. At some critical heads, the Q values plateaued and did not increase any further with increasing h. This was attributed to the fact that the maximum available Q provided by the river was achieved with no further possible increase, regardless of the head. This indicates that the Q values given by the model were an upper limit. In addition, this plateau point at which the modeled and experimental values deviated can be used as an indicator of the maximum achievable flow under a specific set of practical operating conditions. In the case of energy generation, this indicator could be used to identify the maximum possible power in a particular season, thereby providing useful site-specific information to design and operate full-scale systems.

The proposed model was compared with other similar models (Ackers and Crump, 1960; Hager, 1985; Mulligan et al., 2016; Pica, 1970) and relevant experimental data under large-scale vortex drop conditions (d = 5.5 m, b = 5.5 m, and R_i = 8.3 m) (Drioli, 1969). All datasets were reproduced from Mulligan et al. (2016), who presented a detailed discussion on the differences of these models. Briefly, most of these models are semi-analytical, with some empirical relationships or use of experimental data as model inputs. The depth−discharge curves in Fig. 5 clearly show that all the compared models provided a similar trend, although the reported values varied. The large scatter indicates that none of the models reproduced the experimental dataset well. As the

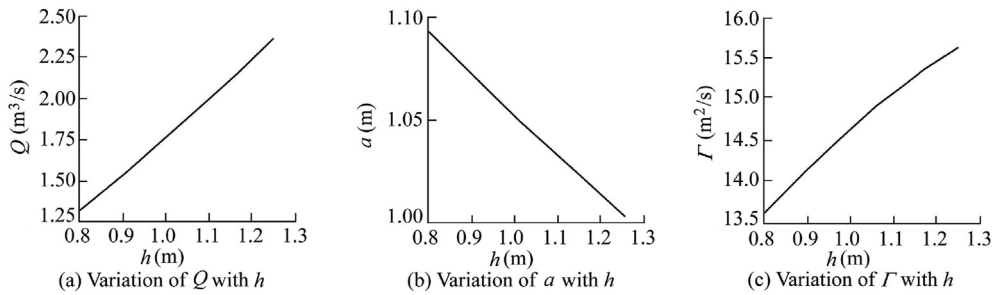

(a) Variation of Q with h (b) Variation of a with h (c) Variation of Γ with h

Fig. 3. Typical analytical results from proposed model.

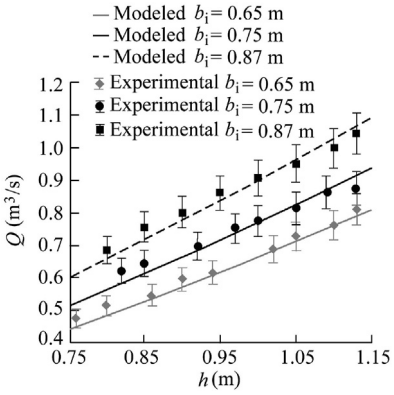

Fig. 4. Experimental verification of proposed model.

details of the experimental conditions and uncertainty of these data are unavailable, it is difficult to conclude which model is superior. Many of these previous models were developed using experimental data and empirical relationships from laboratory-scale measurements, and there are concerns regarding whether such models are scalable. As noted previously (Mulligan et al., 2016), the lack of experimental data for large-scale vortices made it impossible to verify these models. In the prototype presented by Drioli (1969) and the GVHP system in this study, very high Reynolds numbers of approximately 10^6 to 10^7 were encountered, which were much higher than those in laboratory systems. It should be noted that the turbulent effects on the vortex flow in full-scale systems may produce behavior that cannot be accurately described by the models verified using the empirical data from laboratory-scale physical models (Mulligan et al., 2016). In this study, detailed experimental data for a practical-scale strong free-surface vortex system, which are not available in the relevant literature, were provided. These data are expected to be useful to further verify existing and future analytical models and to clarify the scaling effects in such systems.

3.2. Sensitivity analysis

Sensitivity analysis was performed to determine the effect of variations of the input parameters on the model outputs.

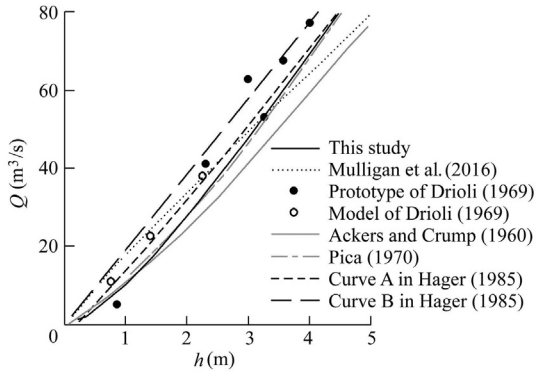

Fig. 5. Comparison of proposed model with selected results from literature.

This is important when the model is used to analyze an existing system with fixed geometric parameters and provides information regarding the output parameter sensitivity to the experimental uncertainties of input parameters. Fig. 6 shows the scatter plots of the model outputs as a function of the fractional variation of each input variable. The initial values of h, b_i, d, and R_i were defined as 1.2 m, 1.2 m, 1.4 m, and 3 m, respectively. These input variables were altered in the ranges of 0.8−1.4 m, 0.8−1.6 m, 1.2−1.6 m, and 2.5−3.5 m, respectively. It was found that most datasets were highly linear, with correlation coefficients exceeding 99%. The relationships between Q and h, a and R_i, and Γ and h shown in Fig. 6 were slightly nonlinear. The corresponding gradients of these curves are listed in Table 1 to quantitatively measure the effect of the variation of individual variables on model outputs. Higher gradients indicate that the variation of the input variable has a more significant effect on the output. Overall, Q was most sensitive to the variation of h, and a 10% uncertainty in the h value resulted in a variation of 13% in Q. However, the variation of h did not significantly affect the other output variables. The effect of d was significant as well. The variation of this input parameter equally affected all output variables, and a and Γ were only significantly sensitive to changes in d. In a full-scale GVHP system, the tank dimensions of d and R_i are usually fixed. As the tank is made from concrete or steel, these dimensions are expected to remain stable and can be measured with a high degree of precision (< 0.5%) when the tank is dry. Although some systems have a mechanism for varying b_i, an optimized b_i value is usually chosen, and this value is also fixed after the initial test. Therefore, the only dynamic input variable is the water head. As the experimental results in this study showed that h can be measured with a precision of 1%, its effect on the simulated Q was within an acceptable margin of uncertainty. It is interesting to note that the geometrical parameters of the circulation tank (d, b_i, and R_i) had an identical effect on a and Γ.

The proposed model provides several advantages for the analysis and design of practical strong free-surface vortex flows. For existing systems with fixed geometrical parameters, this model can be used to provide the depth−discharge relationship (i.e., the maximum Q as a function of h). In the case of hydropower systems, this Q value can be used to calculate the maximum theoretical power output. Γ is a very important parameter for energy dissipation or energy generation applications. However, this parameter is difficult to accurately measure. The proposed model can provide the Γ value for hydropower systems. Specifically, a velocity profile of the vortex can be determined from Γ, which is useful for turbine design in hydropower systems. In addition, the model is valuable for the design of new vortex-based systems, through which the geometrical parameters can be optimized to achieve the desired Q and Γ values for practical applications. For example, the dimensions of the circulation tank and channels can be optimized for efficient material utilization to reduce construction costs.

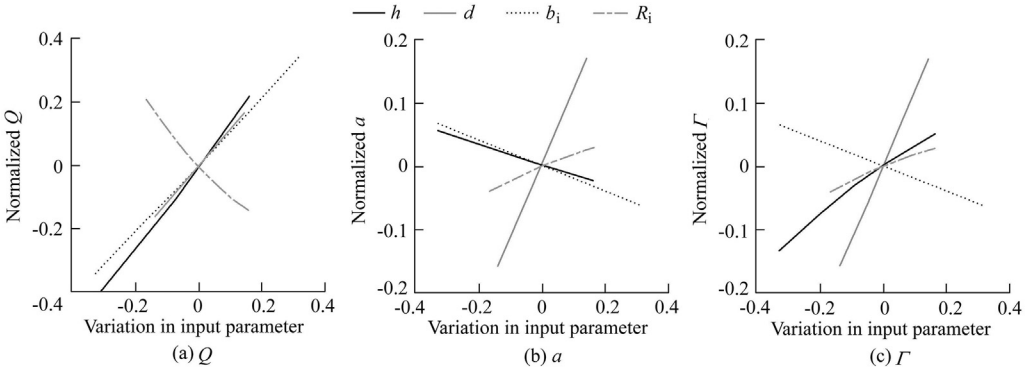

Fig. 6. Results of sensitivity analyses.

Table 1
Gradients of sensitivity plots shown in Fig. 6.

Model output	Input variable			
	h	b_i	d	R_i
Q	**1.305**	1.048	1.157	−1.072
a	−0.170	−0.200	**1.159**	0.203
Γ	0.382	−0.200	**1.159**	0.203

Note: Values in bold denote the maximum gradients for each model output.

4. Conclusions

In this study, an analytical model was established to describe strong free-surface vortex flow. This model can accurately describe the depth−discharge relationship of a full-scale vortex. The main conclusions can be summarized as follows:

(1) The proposed model agreed with the experimental data within experimental uncertainty. Hence, we consider that the model is sufficiently validated for practical-scale vortex systems. Unlike most previous models, which were validated using laboratory-scale physical models, or a few isolated data points, our model was verified over a wide range of operating conditions of a practical-scale system.

(2) This study obtained experimental depth−discharge curves over a range of inlet-width conditions to address the lack of experimental data in the literature for practical-scale vortices. The versatile model presented in this study and the detailed experimental data are expected to be highly useful for analysis of the scalability of existing models that have been previously verified using laboratory-scale physical models.

(3) Unlike existing models, a major advantage of the proposed model is that the volumetric flow rate is not required as a model input. This advantage allows the model to be easily applied to the analysis of existing vortex systems with fixed geometries and the design of new systems. In addition, this model does not use the assumption of a constant velocity across the vortex radius, which allows the precise calculation of the locations of resultant tangential velocity vectors. In the case of energy generation systems such as GVHP, this could be highly valuable for turbine design because the inlet and outlet velocity triangles are highly correlated with the generated power. Given that low turbine efficiency is considered a major limitation of the GVHP system, future studies will focus on using this model to design an optimized turbine for this system.

Declaration of competing interest

The authors declare no conflicts of interest.

References

Ackers, P., Crump, E.S., 1960. The vortex drop. Proc. Inst. Civ. Eng. 16(4), 433−442. https://doi.org/10.1680/iicep.1960.11720.

Alzamora Guzmán, V.J., Glasscock, J.A., Whitehouse, F., 2019. Design and construction of an off-grid gravitational vortex hydropower plant : A case study in rural Peru. Sust. Energy Technol. Assess. 35, 131−138. https://doi.org/10.1016/j.seta.2019.06.004.

Bansal, R.K., 2010. A Textbook of Fluid Mechanics and Hydraulic Machines, ninth ed. Laxmi Publication Pty. Ltd., New Delhi.

Dhakal, R., Chaulagain, R.K., Bajracharya, T., Shrestha, S., 2015. Economic feasibility study of gravitational water vortex power plant for the rural electrification of low head region of Nepal and its comparative study with other low head power plant. In: Proceedings of the 11th International Conference ASIAN Community Knowledge Networks for the Economy, Society, Culture, and Environmental Stability. Kathmandu, pp. 127−135. https://doi.org/10.13140/RG.2.1.4383.4483.

Drioli, C., 1969. Esperienze su installazioni con pozzo di scarico a vortice. Energia Elettr. 66, 399−409 (in Italian).

Hager, W.H., 1985. Head-discharge relation for vortex shaft. J. Hydraul. Eng. 111(6), 1015−1020. https://doi.org/10.1061/(ASCE)0733-9429(1985)111:6(1015).

Khan, N., 2016. Blade Optimization of Gravitational Water Vortex Turbine. Ph. D. Dissertation. Ghulam Ishaq Khan Institute of Engineering Sciences and Technology, Khyber Pakhtunkhwa.

Knauss, J.E., 1987. Swirling Flow Problems at Intakes. CRC Press/Balkema, Leiden.

Kouris, P.S., 2000. Hydraulic Turbine Assembly. US Patent US006114773A.

Kueh, T.C., Beh, S.L., Rilling, D., Ooi, Y., 2014. Numerical analysis of water vortex formation for the water vortex power plant. Int. J. Innov. Manag. Technol. 5(2), 111−115. https://doi.org/10.7763/IJIMT.2014.V5.496.

Li, H.F., Chen, H.X., Ma, Z., Yi, Z., 2008. Experimental and numerical investigation of free surface vortex. J. Hydrodyn. 20(4), 485−491. https://doi.org/10.1016/S1001-6058(08)60084-0.

Mulligan, S., 2015. Experimental and Numerical Analysis of Three-Dimensional Free-Surface Turbulent Vortex Flows with Strong Circulation. Ph. D. Dissertation. IT Sligo, Sligo.

Mulligan, S., Casserly, J., Sherlock, R., 2015. Experimental modelling of flow in an open channel vortex chamber. In: E-Proceedings of the 36th IAHR World Congress. The Hague, pp. 1−12.

Mulligan, S., Casserly, J., Sherlock, R., 2016. Effects of geometry on strong free-surface vortices in subcritical approach flows. J. Hydraul. Eng. 142(11), 04016051. https://doi.org/10.1061/(ASCE)HY.1943-7900.0001194.

Mulligan, S., Creedon, L., Casserly, J., Sherlock, R., 2018. An improved model for the tangential velocity distribution in strong free-surface vortices: An experimental and theoretical study. J. Hydraul. Res. 57(4), 547−560. https://doi.org/10.1080/00221686.2018.1499050.

Nishi, Y., Inagaki, T., 2017. Performance and flow field of a gravitation vortex type water turbine. Int. J. Rotating Mach. 2610508. https://doi.org/10.1155/2017/2610508, 2017.

Pica, M., 1970. Scaricatori a vortice. Energia Elettr. 47, 1−18 (in Italian).

Power, C., McNabola, A., Coughlan, P., 2016. A parametric experimental investigation of the operating conditions of gravitational vortex hydropower (GVHP). J. Clean Energy Technol. 4(2), 112−119. https://doi.org/10.7763/JOCET.2016.V4.263.

Rahman, M., Hong, T., Tang, R., Sung, L., Tamiri, F.B.M., 2016. Experimental study the effects of water pressure and turbine blade lengths and numbers on the model free vortex power generation system. Int. J. Current Trends in Eng. Res. 2(9), 13−17.

Rankine, W.J.M., 1872. A Manual of Applied Mechanics. Charles Griffin and Company, Glasgow.

Sritram, P., Treedet, W., Suntivarakorn, R., 2015. Effect of turbine materials on power generation efficiency from free water vortex hydro power plant. In: Proceedings of the 4th Global Conference on Materials Science and Engineering (CMSE 2015). University of Macau-new campus. https://doi.org/10.1088/1757- 899X/103/1/012018.

Tao, T., 2011. An Introduction to Measure Theory. American Mathematical Society, Providence.

Timilsina, A.B., Mulligan, S., Bajracharya, T.R., 2018. Water vortex hydropower technology: A state-of-the-art review of developmental trends. Clean Technol. Environ. Policy 20(8), 1737−1760. https://doi.org/10.1007/s10098-018-1589-0.

Turbulent, 2020. Turbulent Company Website. https://www.turbulent.be/ [Retrieved Feb. 2, 2020].

Vatistas, G.H., Panagiotakakos, G.D., Manikis, F.I., 2015. Extension of the n-vortex model to approximate the effects of turbulence. J. Aircraft 52(5), 1721−1725. https://doi.org/10.2514/1.C033238.

Vorteco, 2016. Water Vortex Power Plants: Ecological Power Technology. http://www.vorteco.com/index_htm_files/Prosp-vortecoA4e8_140313.pdf [Retrieved Dec. 16, 2016].

Wanchat, S., Suntivarakorn, R., 2011. Preliminary design of a vortex pool for electrical generation. Adv. Sci. Lett. 13(1), 173−177. https://doi.org/10.1166/asl.2012.3855.

Zotlöterer, F., 2004. Hydroelectric Power Plant. Patent No. WO 2004/061295 A2.